CHEMICAL PHYSICS

Attosecond dynamics through a Fano resonance: Monitoring the birth of a photoelectron

V. Gruson,[1]* L. Barreau,[1]* Á. Jiménez-Galan,[2] F. Risoud,[3] J. Caillat,[3] A. Maquet,[3] B. Carré,[1] F. Lepetit,[1] J.-F. Hergott,[1] T. Ruchon,[1] L. Argenti,[2]† R. Taïeb,[3] F. Martín,[2,4,5]‡ P. Salières[1]‡

The dynamics of quantum systems are encoded in the amplitude and phase of wave packets. However, the rapidity of electron dynamics on the attosecond scale has precluded the complete characterization of electron wave packets in the time domain. Using spectrally resolved electron interferometry, we were able to measure the amplitude and phase of a photoelectron wave packet created through a Fano autoionizing resonance in helium. In our setup, replicas obtained by two-photon transitions interfere with reference wave packets that are formed through smooth continua, allowing the full temporal reconstruction, purely from experimental data, of the resonant wave packet released in the continuum. In turn, this resolves the buildup of the autoionizing resonance on an attosecond time scale. Our results, in excellent agreement with ab initio time-dependent calculations, raise prospects for detailed investigations of ultrafast photoemission dynamics governed by electron correlation, as well as coherent control over structured electron wave packets.

Tracking electronic dynamics on the attosecond time scale and angstrom length scale is a key to understanding and controlling the quantum mechanical underpinnings of physical and chemical transformations (*1*). One of the most fundamental electronic processes in this context is photoionization, the dynamics of which are fully encoded in the released electron wave packet (EWP) and the final ionic state. The development of broadband coherent sources of attosecond pulses has opened the possibility of investigating these processes with attosecond resolution. On such a short time scale, few techniques (*2*–*5*) are able to provide access to both spectral amplitude and phase. The spectral derivative of the phase, the group delay, is a practical quantity for describing general wave packet properties reflecting the ionization dynamics. Recently, photoemission delays have been measured in a variety of systems: noble gas atoms (*6*–*8*), molecules (*9*), and solids (*10*). In the gas phase, these attosecond delays give insight into the scattering of the electron in the ionic potential; in the solid state, they provide information on the transport dynamics toward the surface. However, the physical relevance of group delays is restricted to fairly unstructured wave packets.

The necessity to go beyond simple delays arises for more complex ionization dynamics when the broadband excitation encompasses continuum structures associated with, for example, autoionizing states, shape resonances, and Cooper minima (*11*–*13*). These structures induce strong spectral variations of the amplitude and phase of the EWP corresponding to different time scales, ranging from the attosecond to the femtosecond domains. In general, the long-term evolution of the EWP amplitude [e.g., the lifetime of Fano autoionizing resonances (*14*)] can be characterized directly in the time domain (*15*), or in the spectral domain with the use of conventional spectroscopic techniques (*16*). However, the EWP phase is required for reconstruction of the full ionization dynamics. In particular, the short-term response associated with broadband excitation remains unexplored (*17*). It is mainly determined by the spectral phase variation over the resonance bandwidth, which has so far not been measured. An additional difficulty is that the characterization techniques often involve strong infrared probe fields that (i) strongly perturb the resonant structures (*18*–*20*) so that the field-free intrinsic dynamics cannot be accessed, and (ii) require elaborate theoretical input for decoding the electron spectrograms (*21*).

Here, we extend attosecond photoionization spectroscopy to the full reconstruction of the time-dependent EWPs produced by coherent broadband excitation through resonant structures. To this end, we have developed a perturbative interferometric scheme enabling the direct measurement of the spectral amplitude and phase of the unperturbed resonant EWP. Interferences between the latter and a reference nonresonant EWP are achieved through two-photon replicas obtained by photoionizing the target with an extreme ultraviolet (XUV) harmonic comb combined with the mid-infrared (MIR) fundamental field. This spectrally resolved technique is easy to implement and offers straightforward access to the EWP characteristics without complex analysis or theoretical input. We apply it to the investigation of the test case of the doubly excited 2s2p autoionizing resonance of helium, for which ab initio time-dependent calculations can be performed (*22*, *23*), thereby providing a benchmark for our experimental study.

Autoionization occurs when a system is excited in structured spectral regions where resonant states are embedded into a continuum. The system can then either directly ionize or transiently remain in the resonant bound state before ionizing. Coupling between the resonant state and continuum states of the same energy through configuration interaction leads to the well-known Fano spectral line shapes (*14*). Of particular interest is the autoionization decay from doubly excited states (*16*) that is a direct consequence of the electron-electron repulsion. Using our spectrally resolved technique, we directly access the complete ionization dynamics (including interferences at birth time) and monitor the resonance buildup on a subfemtosecond time scale—an endeavor of attosecond science (*17*, *24*).

The concept of the method is shown in Fig. 1A. We photoionize helium with a comb of mutually coherent odd harmonics derived from an optical parametric amplifier (OPA) MIR source. The harmonic of order 63 (H_{63}) is driven into the 2s2p resonance, at 60.15 eV from the ground state, by tuning the OPA central wavelength λ_{OPA} to 1295 nm. Because the harmonic width (400 meV) is much larger than the resonance width (Γ = 37 meV), a broad resonant EWP with complex spectral amplitude $A_R(E)$ is produced. Simultaneously, nonresonant EWPs are created by the neighboring harmonics H_{61} and H_{65} in smooth regions of the continuum; each of these can serve as a reference, denoted $A_{NR}(E)$, to probe the resonant EWP.

To induce interference, we use two-photon transitions to create replicas that spectrally overlap with each other. A weak fraction of the fundamental MIR pulse, of angular frequency $\omega_0 = 2\pi c/\lambda_{OPA}$, is superimposed on the harmonic comb with a delay τ. Its intensity (~2×10^{11} W/cm^2) is sufficiently high to induce perturbative two-photon XUV-MIR transitions but is low enough to avoid transitions involving more than one MIR photon [e.g., depletion of the doubly excited state by multiphoton ionization (*15*), or distortion of the resonance line shape (*19*)]. Most important, the MIR spectral width (26 meV) is smaller than both the harmonic and resonance widths, ensuring that each EWP produced in the two-photon process is a faithful, spectrally shifted, replica of the unperturbed EWP produced in

[1]LIDYL, CEA, CNRS, Université Paris-Saclay, CEA Saclay, 91191 Gif-Sur-Yvette, France. [2]Departamento de Química, Módulo 13, Universidad Autónoma de Madrid, 28049 Madrid, Spain. [3]Sorbonne Université, UPMC Université Paris 6, UMR 7614, Laboratoire de Chimie Physique-Matière et Rayonnement, 75231 Paris Cedex 05, France, and CNRS, UMR 7614, LCPMR, Paris, France. [4]Instituto Madrileño de Estudios Avanzados en Nanociencia (IMDEA-Nanociencia), Cantoblanco, 28049 Madrid, Spain. [5]Condensed Matter Physics Center (IFIMAC), Universidad Autónoma de Madrid, 28049 Madrid, Spain.
*These authors contributed equally to this work. †Present address: Department of Physics and CREOL, University of Central Florida, Orlando, FL 32816, USA. ‡Corresponding author. Email: fernando.martin@uam.es (F.M.); pascal.salieres@cea.fr (P.S.)

the XUV one-photon process. Because of the frequency relation between the odd-harmonic XUV comb and the fundamental MIR laser, the resonant EWP upshifted by absorption of a MIR photon, $A_{R+1}(\tau, E + \hbar\omega_0) \propto A_R(E) \exp(i\omega_0\tau)$, and the reference EWP downshifted by stimulated emission of a MIR photon, $A_{NR-1}(\tau, E + \hbar\omega_0) \propto A_{NR}(E + 2\hbar\omega_0) \exp(-i\omega_0\tau)$, coherently add up in the single sideband (SB_{64}) that lies between the lines associated with H_{63} and H_{65}. Similarly, the resonant EWP downshifted by emission of a MIR photon interferes in sideband SB_{62} with the EWP upshifted by absorption of a MIR photon from H_{61}. We designate E the photoelectron energy in the resonant EWP, and $\overline{E} = E \pm \hbar\omega_0$ the photoelectron energy of the resonant EWP replicas in SB_{64} and SB_{62}, respectively.

The spectrum of these sidebands is thus modulated by the interference between the resonant and nonresonant replicas, depending on the XUV-MIR delay τ (*25*). For SB_{64}, the spectrum is given by

$$\begin{aligned} S_{64}(\tau,\overline{E}) &= |A_{R+1}(\tau,\overline{E}) + A_{NR-1}(\tau,\overline{E})|^2 \\ &= |A_{R+1}(\overline{E})|^2 + |A_{NR-1}(\overline{E})|^2 + \\ &\quad 2|A_{R+1}(\overline{E})||A_{NR-1}(\overline{E})| \\ &\quad \times \cos[2\omega_0\tau + \Delta\varphi_{64}(\overline{E}) + \Delta\eta_{scat}(\overline{E})] \end{aligned} \quad (1)$$

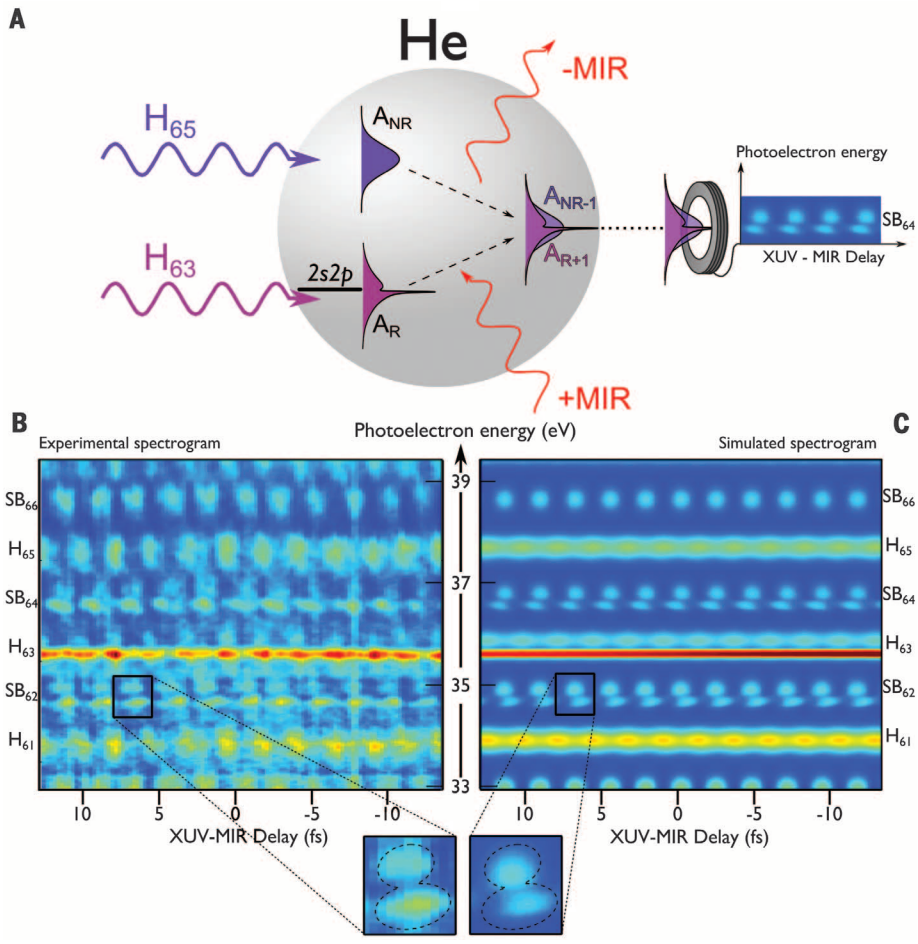

Fig. 1. Principle and resulting spectrogram of spectrally resolved attosecond electron interferometry for the complete characterization of resonant EWPs. (**A**) Principle of the electron interferometry technique. Resonant A_R and reference nonresonant A_{NR} EWPs are produced by successive coherent harmonics. Replicas of these EWPs are created at the same final energy by two-photon transitions induced by a weak fundamental MIR field, where the atom absorbs a MIR photon, leading to the A_{R+1} EWP, or emits a MIR photon, leading to the A_{NR-1} EWP. The spectrally resolved interferences are measured in a time-of-flight electron spectrometer as a function of the XUV-MIR delay τ, controlled with interferometric accuracy; these interferences provide access to the spectral phase of the resonant A_R EWP. (**B** and **C**) Experimental spectrogram (B) and theoretical spectrogram (C) in the 33- to 39-eV region for a 1295-nm OPA wavelength (*25*). H_{63} overlaps the 2s2p resonance of helium located 60.15 eV above the ground state (E_R = 35.55 eV). Single-photon ionization by the odd harmonic orders results in main lines spaced by twice the MIR photon energy, $2\hbar\omega_0$ = 1.92 eV. Between these lines appear sidebands corresponding to two-photon ionization. The oscillations of the two sidebands on both sides of the resonant H_{63} (i.e., SB_{62} and SB_{64}) encode the spectral phase of the resonant EWP. A close-up of one SB_{62} beating shows the structured shape of this resonant EWP and the dephasing of the oscillations of the different spectral components.

where the two contributions to the replicas' relative phase are (i) $2\omega_0\tau$, the phase introduced by the absorption or simulated emission of the MIR photon, and (ii) the relative phase between the initial one-photon EWPs. The latter is split into $\Delta\varphi_{64}(\overline{E}) = \varphi_{65}(\overline{E} + \hbar\omega_0) - \varphi_{63}(\overline{E} - \hbar\omega_0)$, the phase difference between the two ionizing harmonics, and $\Delta\eta_{scat}(\overline{E}) = \eta_{scat}(\overline{E} + \hbar\omega_0) - \eta_{scat}(\overline{E} - \hbar\omega_0)$, the difference between the nonresonant and resonant scattering phases of the two intermediate states. In our conditions, the variations over the sideband width of both $\Delta\varphi_{64}(\overline{E})$ and $\eta_{scat}(\overline{E} + \hbar\omega_0)$ are negligible in comparison with that of the resonant scattering phase $\eta_{scat}(\overline{E} - \hbar\omega_0)$ (*25*). The latter contains information about the scattering of the photoelectron by the remaining core, including strongly correlated scattering by the other electron close to the resonance. This phase is the measurable quantity addressed by our study.

Using a high-resolution (~1.9%) magnetic-bottle spectrometer with a length of 2 m, we have access to the photoelectron spectrogram—electron yield as a function of energy E and delay τ—spectrally resolved within the harmonics and sideband widths (Fig. 1B). As a result of its large bandwidth, H_{63} produces a photoelectron spectrum exhibiting a double structure with a Fano-type resonant peak and a smoother peak. This shape is replicated on each of the closest resonant sidebands (SB_{62} and SB_{64}). Strikingly, the components of the double structure oscillate with different phases when τ is varied, in both SB_{62} and SB_{64}.

These phase variations are further evidenced by a spectrally resolved analysis: For each sampled energy within the sideband width, we perform a Fourier transform of $S_{63\pm1}(\tau, E + \hbar\omega_0)$ with respect to τ to extract the amplitude and phase of the component oscillating at $2\omega_0$ (see Eq. 1 and Fig. 2). The SB_{62} phase shows a strong increase of ~1 rad within the resonant peak, followed by a sudden drop at the amplitude minimum ($\overline{E}$ ~ 34.75 eV), and a rather flat behavior under the smooth peak. The SB_{64} phase has a very similar shape and magnitude but with an opposite sign due to opposite configuration of the resonant and reference EWPs in the interferometer. This correspondence confirms the direct imprint of the intermediate resonance on the neighboring sidebands.

The $2\omega_0$ component of the resonant sidebands thus provides a good measure of the $|A_R(E)| \exp[i\eta_{scat}(E)]$ EWP that would result from one-photon Fourier-limited excitation. This allows a detailed study of the temporal characteristics of resonant photoemission, in particular of the electron flux into the continuum, through the direct reconstruction of this EWP in the time domain:

$$\tilde{A}_R(t) = \frac{1}{2\pi}\int_{-\infty}^{+\infty} |A_R(E)| \exp[i\eta_{scat}(E)] \exp\left(\frac{-iEt}{\hbar}\right) dE \quad (2)$$

The temporal profile obtained from SB_{64} is shown in Fig. 3A. It presents a strong peak at the

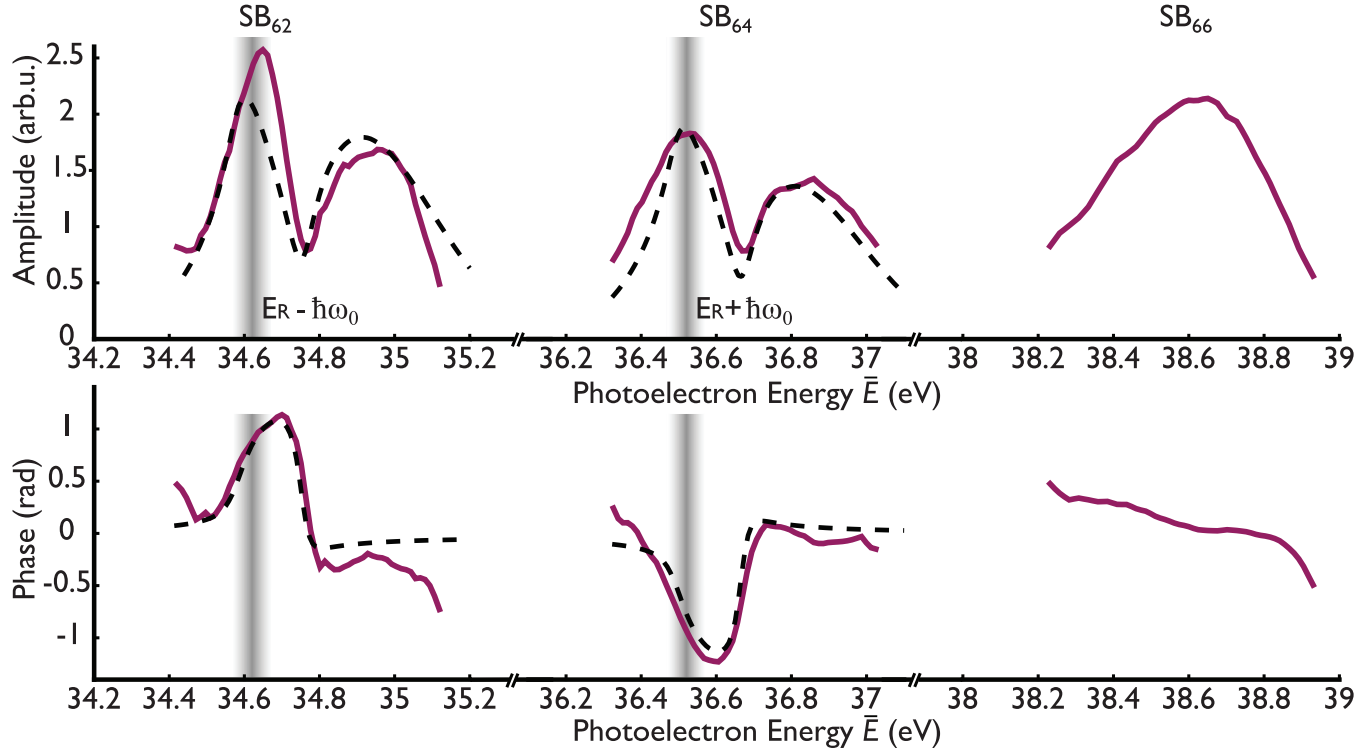

Fig. 2. Resonant EWP in the spectral domain. Upper and lower panels respectively show spectral amplitude and phase of the $2\omega_0$ component of SB_{62} (left), SB_{64} (center), and SB_{66} (right) from the spectrograms in Fig. 1, B and C. The phase origin is set to 0 by removing the linear variation due to the ionizing harmonic radiation (attochirp) (*30*). The experimental data (purple curves) show very good agreement with the simulations (dashed black lines). The resonance position shifted by one MIR photon is indicated in gray. The measured spectral amplitudes and phases of the resonant SB_{62} and SB_{64} are easily related to the amplitude $|A_R(E)|$ and phase $\eta_{scat}(E)$ of the resonant one-photon EWP (see Eq. 1). The main limitation comes from the current spectrometer resolution (in our conditions, a relative resolution of ~1.9% resulting in a width of ~190 meV at 10 eV) that broadens the resonant peak and its phase variations. The nonresonant SB_{66} exhibits a Gaussian amplitude (which mostly reflects the ionizing XUV spectral profile) and a smooth close-to-linear phase. This provides a temporal reference for the ionization dynamics.

origin—given by the maximum of the Fourier transform of the nonresonant SB_{66} (*25*)—followed by a deep minimum around 4 fs and then a revival with a decay within ~10 fs. The presence of a fast phase jump (~2 rad within ~2 fs) at the position of the minimum indicates that it results from a destructive interference between two wave packet components, the origin of which is detailed below.

To benchmark the measured data, we theoretically investigated the multicolor XUV + MIR ionization of He in the vicinity of the 2s2p resonance. Fully correlated ab initio time-dependent calculations (*22*) were used to validate an analytical model of the two-photon transitions accounting for the actual pulses' bandwidths (*23*). The simulated photoelectron spectrogram, taking into account the spectrometer resolution, remarkably reproduces the structured shape of the resonant sidebands as well as the dephasing between their two components (Fig. 1C). The analysis of the $2\omega_0$ oscillations of SB_{62} and SB_{64} gives spectral phase variations in excellent agreement with the experimental data (Fig. 2). The temporal profile $\tilde{A}_R(t)$ obtained by Fourier transform (Fig. 3) is also well reproduced, with a smaller revival but a similar decay time of ~10 fs. This reduced effective lifetime is a direct consequence of the finite spectrometer resolution. When the latter is assumed infinite, the time profile has the same behavior at short times but a longer decay, corresponding to the 17-fs lifetime of the resonance. Analytical calculations show that in our conditions, the reconstructed EWP does mirror the one-photon resonant EWP (*25*). These findings confirm that, except for a faster decay of the long-term tail due to our current electron spectrometer resolution, the essential physics of the early time frame of EWP creation is directly accessed from purely experimental data.

To further highlight the insight provided by this experimental technique, we undertook an in-depth analysis of the measured EWP characteristics in terms of Fano's formalism for autoionization (*14*). Resonant ionization can be described as the interference between two distinct paths: (i) the direct transition to the continuum, and (ii) the resonant transition through the doubly excited state that eventually decays in the continuum through configuration interaction within the resonance lifetime (Fig. 3B). The normalized total transition amplitude can then be written as the coherent sum of two contributions, a constant background term and a Breit-Wigner amplitude for the resonance:

$$R(E) = \frac{\varepsilon + q}{\varepsilon + i} = 1 + \frac{q - i}{\varepsilon + i} \qquad (3)$$

where $\varepsilon = 2(E - E_R)/\Gamma$ is the reduced energy detuning from the resonance at energy E_R, in units of its half width $\Gamma/2$. The Fano parameter q [−2.77 for the He(2s2p) resonance (*16*)] measures the relative weight of the two paths. Their interference leads to the well-known asymmetric Fano line shape $|R(E)|^2$ and to the resonant scattering phase: $\eta_{scat}(E) = \arg R(E) = \mathrm{atan}(\varepsilon) + \pi/2 - \pi\Theta(\varepsilon + q)$, where Θ is the Heaviside function. This phase is experimentally accessed here (Fig. 2).

The spectral amplitude of an EWP created by Gaussian harmonic excitation $H(E)$ is given by $R(E)H(E)$. Its temporal counterpart is $\tilde{A}_R(t) = [\tilde{R} * \tilde{H}](t)$, where $\tilde{R}(t)$ and $\tilde{H}(t)$ are Fourier transforms of the spectral amplitudes, in particular

$$\tilde{R}(t) = \delta(t) - i\frac{\Gamma}{2\hbar}(q - i)\exp\left[-\left(\frac{iE_R}{\hbar} + \frac{\Gamma}{2\hbar}\right)t\right]\Theta(t) \qquad (4)$$

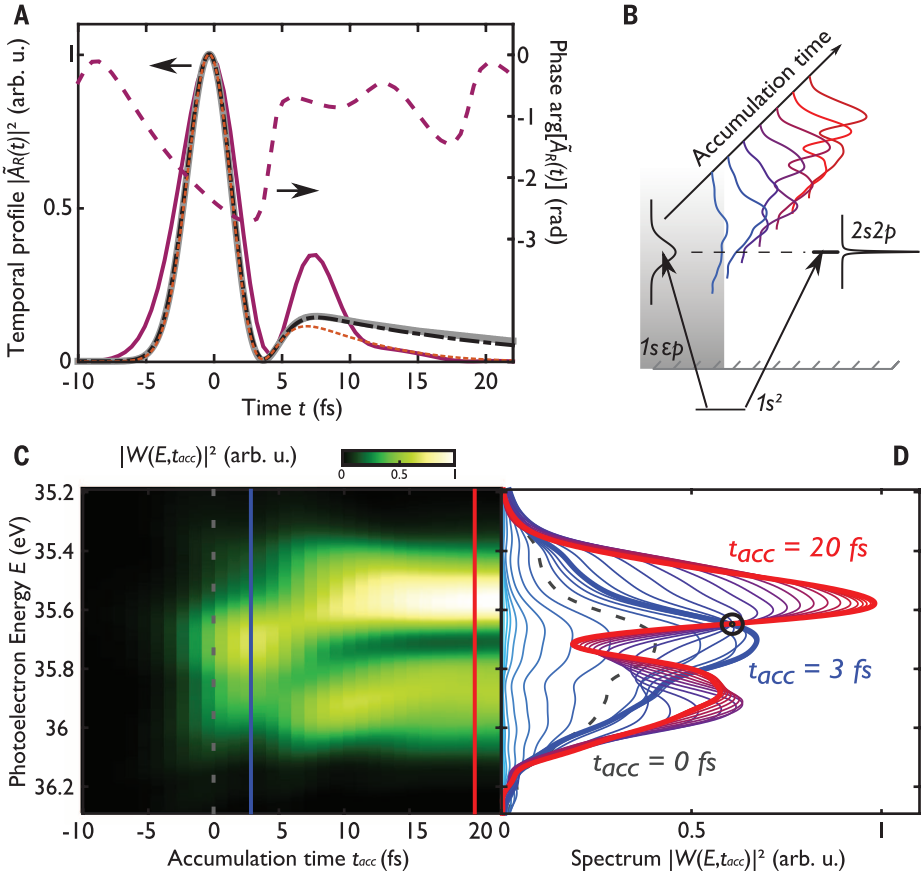

Fig. 3. Resonant EWP in the time domain and time-resolved reconstruction of the resonance buildup. (**A**) Temporal profile of the resonant EWP obtained by Fourier transform of the SB_{64} data (i) from the experimental spectrogram (solid purple curve) and corresponding temporal phase (dashed purple curve), and (ii) from the simulated spectrogram, taking into account (dotted orange curve), or not (dot-dashed black curve), the finite spectrometer resolution. The latter fully coincides with the one-photon resonant EWP profile from a direct analytical calculation (solid gray curve) (*25*), thereby demonstrating the validity of our interferometric technique. (**B**) Illustration of the formation dynamics of the resonant spectrum resulting from interference between the two paths in the Fano autoionization model. (**C**) Reconstruction of the time-resolved buildup of the resonant spectrum using the time-energy analysis introduced in Eq. 5. The photoelectron spectrum is plotted as a function of the upper temporal limit (accumulation time t_{acc}) used for the inverse Fourier transform. The dashed gray curve, solid blue curve, and solid red curve indicate accumulation times of 0, 3, and 20 fs, respectively. (**D**) Lineouts of (C) every 1 fs. This figure evidences first the growth of the direct path until a maximum is reached at ~3 fs (blue curves), and then the increasing spectral interference with the resonant path that finally results in the Fano line shape (red curves). At 35.6 eV, an isosbestic-like point is crossed by all curves from 3 fs onward (black circle), evidencing a position in the final line shape where only the direct path contributes.

(*24*). The temporal profile $\tilde{A}_R(t)$ thus decomposes into a Gaussian nonresonant term and a resonant contribution, like our experimental data (Fig. 3A). The destructive temporal interference between the two terms leads to the amplitude minimum and phase jump identified around t = 4 fs.

To illustrate how the interference between the two paths governs the formation of the resonance line shape, Wickenhauser *et al.* (*17*) introduced a time-frequency analysis based on the limited inverse Fourier transform:

$$W(E,t_{acc}) = \int_{-\infty}^{t_{acc}} \tilde{A}_R(t) \exp\left(\frac{iEt}{\hbar}\right) dt \qquad (5)$$

which shows how the spectrum builds up until accumulation time t_{acc}. The result of this transform applied to the experimental EWP in Fig. 3A is shown in Fig. 3, C and D. The chronology of the resonance formation can be nicely interpreted within Fano's formalism. In a first stage until ~3 fs, a close-to-Gaussian spectrum reflecting the ionizing harmonic spectral shape emerges: The direct path to the continuum dominates. Then the resonant path starts contributing as the populated doubly excited state decays in the continuum: Interferences coherently build up until ~20 fs, consistent with the temporal profile in Fig. 3A, to eventually converge toward the asymmetric measured spectrum. The resonance growth can thus be decomposed in two nearly consecutive steps governed by fairly different time scales.

The buildup of the resonant profile reveals the presence of a notable point around E = 35.6 eV where, as soon as the direct ionization is completed, the spectrum barely changes with t_{acc} any longer. This can be explained by splitting the $|R(E)|^2$ spectrum from Eq. 3 into three terms:

$$|R(E)|^2 = 1 + \frac{q^2+1}{\varepsilon^2+1} + 2\frac{q\varepsilon - 1}{\varepsilon^2+1} \qquad (6)$$

(*26*). At this isosbestic-like point—that is, for $\varepsilon = [(1/q) - q]/2$—the bound (second term) and coupling (third term) contributions ultimately cancel each other, leaving only the direct continuum contribution (first term). This point thus gives a useful landmark in the resonant line shape (e.g., for cross section calibration or reference purposes).

Spectrally resolved electron interferometry thus provides insight into the ultrafast strongly correlated multielectron dynamics underlying autoionization decay. Given the generality and wide applicability of the Fano formalism [see, e.g., (*26*)], we anticipate that our approach, combined with progress in attosecond pulse production and particle detection (e.g., access to photoelectron angular distributions), will open prospects for studies of complex photoemission dynamics close to resonances and, more generally, structured EWP dynamics in a variety of systems, from molecules (*27*–*29*) and nanostructures (*26*) to surfaces (*10*). Furthermore, the well-defined amplitude and phase distortions induced by the resonance offer a means for shaping the broadband EWP, bringing opportunities for coherent control in the attosecond regime.

REFERENCES AND NOTES

1. F. Krausz, M. Ivanov, *Rev. Mod. Phys.* **81**, 163–234 (2009).
2. M. Hentschel *et al.*, *Nature* **414**, 509–513 (2001).
3. P. M. Paul *et al.*, *Science* **292**, 1689–1692 (2001).
4. Y. Mairesse, F. Quéré, *Phys. Rev. A* **71**, 011401(R) (2005).
5. M. Chini, S. Gilbertson, S. D. Khan, Z. Chang, *Opt. Express* **18**, 13006–13016 (2010).
6. M. Schultze *et al.*, *Science* **328**, 1658–1662 (2010).
7. K. Klünder *et al.*, *Phys. Rev. Lett.* **106**, 143002 (2011).
8. R. Pazourek, S. Nagele, J. Burgdörfer, *Rev. Mod. Phys.* **87**, 765–802 (2015).
9. S. Haessler *et al.*, *Phys. Rev. A* **80**, 011404 (2009).
10. A. L. Cavalieri *et al.*, *Nature* **449**, 1029–1032 (2007).
11. S. B. Schoun *et al.*, *Phys. Rev. Lett.* **112**, 153001 (2014).
12. M. Sabbar *et al.*, *Phys. Rev. Lett.* **115**, 133001 (2015).
13. M. Kotur *et al.*, *Nat. Commun.* **7**, 10566 (2016).
14. U. Fano, *Phys. Rev.* **124**, 1866–1878 (1961).
15. S. Gilbertson *et al.*, *Phys. Rev. Lett.* **105**, 263003 (2010).
16. M. Domke, K. Schulz, G. Remmers, G. Kaindl, D. Wintgen, *Phys. Rev. A* **53**, 1424–1438 (1996).
17. M. Wickenhauser, J. Burgdörfer, F. Krausz, M. Drescher, *Phys. Rev. Lett.* **94**, 023002 (2005).
18. Z.-H. Loh, C. H. Greene, S. R. Leone, *Chem. Phys.* **350**, 7–13 (2008).
19. C. Ott *et al.*, *Science* **340**, 716–720 (2013).
20. C. Ott *et al.*, *Nature* **516**, 374–378 (2014).

21. S. R. Leone *et al.*, *Nat. Photonics* **8**, 162–166 (2014).
22. Á. Jiménez-Galán, L. Argenti, F. Martín, *Phys. Rev. Lett.* **113**, 263001 (2014).
23. A. Jiménez-Galán, F. Martín, L. Argenti, *Phys. Rev. A* **93**, 023429 (2016).
24. Z. X. Zhao, C. D. Lin, *Phys. Rev. A* **71**, 060702 (2005).
25. See supplementary materials on *Science* Online.
26. A. E. Miroshnichenko, S. Flach, Y. S. Kivshar, *Rev. Mod. Phys.* **82**, 2257–2298 (2010).
27. A. S. Sandhu *et al.*, *Science* **322**, 1081–1085 (2008).
28. J. Caillat *et al.*, *Phys. Rev. Lett.* **106**, 093002 (2011).
29. P. Hockett, E. Frumker, D. M. Villeneuve, P. B. Corkum, *J. Phys. B* **49**, 095602 (2016).
30. Y. Mairesse *et al.*, *Science* **302**, 1540–1543 (2003).

ACKNOWLEDGMENTS

We thank S. Weber for crucial contributions to the PLFA attosecond beamline; D. Cubaynes, M. Meyer, F. Penent, and J. Palaudoux for setup and testing of the electron spectrometer; and O. Smirnova for fruitful discussions. Supported by European Union grant H2020-MSCA-ITN-MEDEA-641789, Agence Nationale de la Recherche grants ANR-15-CE30-0001-01-CIMBAAD and ANR11-EQPX0005-ATTOLAB, European Research Council advanced grant XCHEM 290853, European COST Action grant XLIC CM1204, and MINECO Project grant FIS2013-42002-R. We acknowledge allocation of computer time from CCC-UAM and Mare Nostrum BSC.

SUPPLEMENTARY MATERIALS

www.sciencemag.org/content/354/6313/734/suppl/DC1
Supplementary Text
Figs. S1 to S7
Movie S1
References (*31*–*43*)

8 July 2016; accepted 5 October 2016
10.1126/science.aah5188

CHEMICAL PHYSICS

Observing the ultrafast buildup of a Fano resonance in the time domain

A. Kaldun,[1]*† A. Blättermann,[1]† V. Stooß,[1] S. Donsa,[2] H. Wei,[3] R. Pazourek,[2] S. Nagele,[2] C. Ott,[1] C. D. Lin,[3] J. Burgdörfer,[2] T. Pfeifer[1,4]‡

Although the time-dependent buildup of asymmetric Fano line shapes in absorption spectra has been of great theoretical interest in the past decade, experimental verification of the predictions has been elusive. Here, we report the experimental observation of the emergence of a Fano resonance in the prototype system of helium by interrupting the autoionization process of a correlated two-electron excited state with a strong laser field. The tunable temporal gate between excitation and termination of the resonance allows us to follow the formation of a Fano line shape in time. The agreement with ab initio calculations validates our experimental time-gating technique for addressing an even broader range of topics, such as the emergence of electron correlation, the onset of electron-internuclear coupling, and quasi-particle formation.

Fano resonances generally occur in the course of excitation of discrete quantum states embedded in and coupled to a continuum (*1*, *2*). As such, they play a fundamental role in nuclear, atomic, molecular, and condensed-matter physics as well as photonics (*3*–*12*). In the prominent example of helium, the discrete doubly excited states are located within different sets of continua, where the prominent 2s2p state is coupled only to the continuum of singly ionized ground-state Helium He^+ (1s). Coulomb interaction among the two electrons leads to autoionization, thus coupling the discrete state and the 1s continuum and giving rise to the famous asymmetric Fano line profiles. Following the early scientific work on attosecond dynamics in laser-driven helium (*13*, *14*), several recent theoretical calculations have predicted the time-dependent formation of Fano resonances (*15*–*20*). However, up to now no such experiment has been performed.

Here, we report a measurement of the time-dependent formation of a Fano resonance in the prototype system of helium. We observed the transient buildup of the 2s2p doubly excited state via extreme ultraviolet (XUV) absorption spectroscopy using high-harmonic radiation. Monitoring the formation of the Fano line was achieved by rapidly terminating the coherent dipole response of the atom via saturated strong-field ionization (SFI) by use of an intense near-infrared (NIR) laser pulse. The key idea is that the NIR pulse acts as a temporal gate of the Fano resonance decay. By varying the time delay between the XUV and the NIR pulse with subfemtosecond precision, we tracked the evolution of the Fano line shape in real time (Fig. 1). To that end, we used laser intensities beyond the Fano-phase control regime discussed in previous work (*7*) to fully deplete the doubly excited state by means of SFI at variable time delays instead of just shifting its phase at a constant (near zero) time delay.

Although recent theoretical work has concentrated on the photoelectron spectrum for accessing the autoionization process, we made use of the fact that state-of-the-art optical spectrometers (*7*, *21*) attain at least an order of magnitude better energy resolution as compared with that of electron spectrometers (*22*), thus allowing for the observation of subtle changes in the spectral profile.

Upon excitation, the XUV pulse triggers the dynamic buildup of the Fano resonance by inducing an oscillating dipole moment, which in turn gives rise to the optical dipole response of the transition. Signatures in the transmitted XUV spectrum are related to the imaginary part of the frequency-domain dipole response (*7*). The time-delayed strong-field NIR pulse is then used to ionize the system, depleting the autoionizing level and ending the buildup process of the spectral line. The experimental results in Fig. 2 show the time-dependent formation of the 2s2p Fano absorption line. For the unperturbed case—in the absence of the NIR pulse as depicted in Fig. 2 (gray line)—we measured the original Fano line shape. The intensity of the 7-fs full width at half maximum (FWHM) NIR pulse was set high enough (~10^{13} W/cm^2) so that the doubly excited states were completely ionized. The dipole oscillation, and with that the resonant optical response of the atom, was thus terminated within the NIR pulse duration. Because this interruption due to SFI is considerably shorter than the lifetime of the state, we can sample the time-dependent formation of the line shape (*20*). For positive time delays τ, the terminating NIR pulse arrives after the XUV excitation pulse. When τ is small as compared with the state's lifetime of ~17 fs, the short duration in which radiation is emitted by the XUV-triggered dipole oscillation is insufficient to form a well-defined Fano line, as can be seen in Fig. 2 for τ less than 10 fs. At $\tau \approx 6$ fs, the effect of the NIR is strongest, and the spectral line is smeared out completely. When the autoionizing state is immediately depopulated after its excitation, the spectral response is mainly determined by the excitation process driven by the attosecond XUV pulse and, because of the fast termination by the NIR pulse, spans several electron volts. This result agrees with several theoretical studies (*15*, *16*) that show that the energy distribution of the electrons ejected within one third of the state lifetime (corresponding to 6 fs in the case of the 2s2p state in helium) after the initial excitation is governed by the frequency range of the excitation pulse. Now, by increasing the time delay τ between excitation and ionization, the doubly excited state has time to decay, and the interference with the direct contributions builds up; the oscillating dipole is granted more and more time to emit the optical response. This gives rise to a narrower

[1]Max-Planck-Institut für Kernphysik, Saupfercheckweg 1, 69117 Heidelberg, Germany. [2]Institute for Theoretical Physics, Vienna University of Technology, Wiedner Hauptstraße 8, 1040 Vienna, Austria. [3]Department of Physics, Kansas State University, 230 Cardwell Hall, Manhattan, KS 66506, USA. [4]Center for Quantum Dynamics, Universität Heidelberg, 69120 Heidelberg, Germany, EU. *Present address: Stanford PULSE Institute, SLAC National Accelerator Laboratory, 2575 Sand Hill Road, Menlo Park, CA 94025, USA. †These authors contributed equally to this work. ‡Corresponding author. Email: thomas.pfeifer@mpi-hd.mpg.de

Science
AAAS

Attosecond dynamics through a Fano resonance: Monitoring the birth of a photoelectron

V. Gruson, L. Barreau, Á. Jiménez-Galan, F. Risoud, J. Caillat, A. Maquet, B. Carré, F. Lepetit, J.-F. Hergott, T. Ruchon, L. Argenti, R. Taïeb, F. Martín and P. Salières (November 10, 2016)
Science **354** (6313), 734-738. [doi: 10.1126/science.aah5188]

Editor's Summary

Watching as helium goes topsy-turvy

Theorists have long pondered the underpinnings of the Fano resonance, a spectral feature that resembles adjacent rightside-up and upside-down peaks. An especially well-studied instance of this feature appears in the electronic spectrum of helium as a transient state undergoes delayed ionization. Two studies have now traced the dynamics of this state in real time. Gruson *et al.* used photoelectron spectroscopy to extract the amplitude and phase of the electron wave packet after inducing its interference with reference wave packets tuned into resonance at variable delays. Kaldun *et al.* used extreme ultraviolet absorption spectroscopy to probe the transient state while variably forcing ionization with a strong near-infrared field.

Science, this issue pp. 734 and 738

Science (print ISSN 0036-8075; online ISSN 1095-9203) is published weekly, except the last week in December, by the American Association for the Advancement of Science, 1200 New York Avenue NW, Washington, DC 20005.